Article:
Cai, N, Yang, H, Zhang, X et al. (7 more authors) (2020) Bimetallic carbon nanotube encapsulated Fe-Ni catalysts from fast pyrolysis of waste plastics and their oxygen reduction properties. Waste Management, 109. pp. 119-126. ISSN 0956-053X

https://doi.org/10.1016/j.wasman.2020.05.003

Bimetallic Carbon Nanotube Encapsulated Fe-Ni Catalysts from Fast Pyrolysis of Waste Plastics and their Oxygen Reduction Properties

Ning Cai[1,2], Haiping Yang[1*], Xiong Zhang[1], Sunwen Xia[1], Dingding Yao[1], Pietro Bartocci[3], Francesco Fantozzi[3], Yingquan Chen[1], HanpingChen[1], Paul T. Williams[4]

[1]State Key Laboratory of Coal Combustion, School of Energy and Power Engineering, Huazhong University of Science and Technology, 430074 Wuhan, China

[2]China-EU Institute for Clean and Renewable Energy, Huazhong University of Science and Technology, 1037 Luoyu Road, Wuhan, Hubei 430074, China

[3]Department of Engineering, University of Perugia, via G. Duranti 67, 06125, Perugia, Italy

[4]School of Chemical and Process Engineering, University of Leeds, Leeds, LS2 9JT UK

***Corresponding Author:**

Name: Haiping Yang

Tel.: +86 027 87542417x8211

Email addresses: yhping2002@163.com

Postal address: State Key Laboratory of Coal Combustion, Huazhong University of Science and Technology, 1037 Luoyu Road, Wuhan, Hubei 430074, PR China (H.Yang).

Abstract

Carbon-based bimetallic electrocatalystswereobtainedby catalytic pyrolysis of waste plasticswith Fe-Ni-based catalystsand were used asefficient oxygen reduction reaction (ORR) catalysts in this study. The prepared iron-nickel alloy nanoparticles encapsulated in oxidized carbon nanotubes (FeNi-OCNTs) are solid products with a unique structure.Moreover, the chemical composition and structural features of FeNi-OCNTs were determined.The iron-nickel alloy nanoparticleswere wrapped in carbon layers,and the carbon nanotubes had an outer diameterof 20–50 nm and micron-scale lengths.FeNi-OCNT with a Fe/Ni ratio of 1:2 (FeNi-OCNT12)exhibited remarkable electrochemical performance as anORR catalyst with a positive onset potential of 1.01 V(vs. RHE) and a half-wave potential of 0.87 V (vs. RHE),which were comparable to those of a commercial 20% Pt/C catalyst. Furthermore, FeNi-OCNT12 exhibited promising long-term stability and higher tolerance to methanol than the commercial 20% Pt/C catalyst in an alkaline medium. These properties were attributable to the protectiveOCNT coating of the iron-nickel alloy nanoparticles.

Keywords: Waste plastics;Catalytic pyrolysis;bimetallic catalysts; Carbon nanotubes;Oxygen Reduction Reaction.

Nomenclature

ω	Electrode rotation rate	1/s
A	Electrode area	cm^2

As	Ash	wt.%
B	Levich constant	$A/(s)^{0.5}$
CNTs	Carbon nanotubes	-
C_0	Bulk concentration of O_2	mol/cm^3
D_0	Diffusion coefficient	cm^2/s
E	Electrode potential	V
F	Faraday constant	A × s/mol
FC	Fixed carbon	wt.%
J	Measured current density	A
M	Moisture	wt.%
OCNT	Oxidized carbon nanotubes	-
n	Electron transfer number	-
v	Kinetic viscosity of the electrolyte	cm^2/s
V	Volatile matter	wt.%
Pedices		
ar	As received	-
db	Dry basis	-
L	Diffusion-limited current density	-
K	Kinetic current density	-

1 Introduction

Over the last decades, the sharp increase in the demand for plastics resulted in an

estimated annual plastics production of ~400 Mt (380 Mt in 2015) (Geyer et al., 2017), and a consequent growth in the generation of plastic waste, which is currently ~300 Mt per year(Zhao et al., 2018). InChina, it is estimated thatover 70 Mt of plastic waste were producedin 2017(Caroline et al., 2018).While most plastic waste is landfilled or incinerated, and only small amounts are recycled, a significant proportionis discarded indiscriminately, resulting in acute environmental pollution(Sharuddin et al., 2016). Given the challenges in the management of plastic waste, the development of novel processes that enable its conversion into high value products is appealing, as it incentivizes plastic waste recycling(Yao et al., 2018b).

Pyrolysisis a thermal degradation process through whichwaste plastics can be converted into gaseous fuels and liquid products,andit has been considered a promising method inplastic waste management(Bientinesi et al., 2009).And pyrolysis or catalytic pyrolysis process has been proved to be an economical way (S.M. Al-Salem, 2017). Furthermore, the catalytic pyrolysis of waste plasticscan enhance the calorific value of the gas and the concentration of hydrogenand can deliver high-value-added solid products such ascarbon nanotubes (CNTs)(D. Yao et al., 2018; Yao et al., 2018a; Yao et al., 2017). The outstanding physical and chemical properties of CNTsincite research on their extensive applications, such astheir use as electrocatalysts in theORR (oxygen reduction reaction) electrocatalysts. In the preparation ofCNTs by catalytic pyrolysis of waste plastics, the choice of the pyrolysis catalyst not only affects the characteristics of thesolid products but also significantly impacts the stability and electrical conductivity properties of theCNTs(Sharuddin et al., 2016).

At present, iron-(Aboul-Enein et al., 2018; Jonathan et al., 2016) and nickel-based(Ochoa et al., 2017; Wu et al., 2009) catalysts are mainly used in the catalytic pyrolysis of waste plastics. Iron-based catalystscan promote the production of CNTs(Kong et al., 1998; Shen et al., 2014) because of their higher carbon solubility.In contrast, the use of nickel-based catalystscan lead to higher quality of the CNTs due to their ability to cleave C–C and C–H bonds(De et al., 2016; Shen et al., 2014).In previous studies, we found that pyrolysis of waste plastics with an iron-nickel catalyst delivered CNTs in41%yield, which is higher than the yields of iron- (~35%)and nickel-based catalysts (~21%)(Yao et al., 2018a). Moreover, iron- and nickel-based electrocatalystsfind wide applications in electrochemistry. For example, Fe_3C obtained by reforming of hydrocarbons with aniron-based catalyst is an active ORR catalyst(Jiang et al., 2016). However, the low stability of the iron-based electrocatalyst limits its further application. Wu et al. found that a polyaniline–iron–carbon (PANI–Fe–C) electrocatalyst suffered from serious iron sulfide erosion, which led to a decrease in current density of about 50% within 200h(Ferrandon et al., 2013). Nickel is a low-cost metalwith electronic properties which are similar to those of iron, such as the number of electrons and holes in the d-band (Okpalugo et al., 2018), and its reactivity resembles that of palladium or platinum(Stamenkovic et al., 2007), as demonstrated by its use as an alternative to Pt or Pd in the ORR(Lai et al., 2019; Zhao et al., 2015). Furthermore, efficient preparation of Ni-alloyswith most transition metals in different ratios is possible and enables the investigation of the diverse catalytic applications of a wide range of composition-dependent bimetallic nickel systems(De et al., 2016).For

instance, Lai et al.prepared ultrathin multimetallic Pt-Pd-Ni material by a co-reduction method, and the $Pt_{32}Pd_{48}Ni_{20}$ nanosheets exhibited superior catalytic activity to the commercial Pt/C catalyst(Lai et al., 2019). However, studies on the use of bimetallic iron-nickel alloysas ORR electrocatalysts are scarce,and the active sites of carbon-based iron-nickel alloy electrocatalysts remain elusive.

Herein,we report the synthesis of Fe-Nicatalysts, the influence of theFe-Ni loading of oxidized carbon nanotubes (OCNTs) on the electrocatalytic oxygen reduction properties, and detailed mechanistic studies. A highly active and durable catalyst （Fe-Ni-bimetallic-loaded OCNTs）is identified. This work provides a novel strategy to reutilize plastic waste,whilst contributing to the development of low-cost,high-performance non-precious metal catalysts for the ORR.

2 Materials and Methods

2.1 Materials and Chemical Reagents

The employed waste plastic samplesconsisted of used disposable lunch boxes (polypropylene),which were ground toparticles of 0.1–0.5 mm size with a liquid nitrogen grinder.The proximate and ultimate analysis results of the polypropylene waste are presented in Table S1.

Catalyst materials: Nickel nitrate hexahydrate ($Ni(NO_3)_3·6H_2O$), iron nitrate nonahydrate ($Fe(NO_3)_3·9H_2O$), and aluminum oxide (Al_2O_3) were purchased from Sigma Aldrich (China). Absolute ethanol and methanol were purchased from

Sinopharm Chemical Reagent Co. Ltd. (China). 20% Pt/C catalysts and 5% Nafion solution were purchased from Shanghai Hesen Electronics Co. Ltd. (China). All chemicals were analytically pure and used without prior purification.Ultra-pure water (>18 MΩ cm^{-1}) was obtained from a Millipore system and used to prepareall aqueous solutions.All electrochemical measurements were carried out at 25°C.

2.2 Synthesis of Fe-Ni-Al_2O_3Catalysts

Bimetallic Fe-Ni catalysts with different Fe/Ni molarratios were prepared by the impregnation method according to the following procedure:$Fe(NO_3)_3 \cdot 9H_2O$ and $Ni(NO_3)_3 \cdot 6H_2O$ (having different molar ratios 3:1, 2:1, 1:1, 1:2, and 1:3; 1.0 g total mass) were dissolved in 20 mL ethanol, and 10 g γ-Al_2O_3 was addedto eachsolution. The turbidmixtures were stirred for 4 h at 50°C, and subsequently dried in an ovenat 105 °C for 12 h.The dry solids were ground into particles smaller than 0.01 mm andcalcined at 800°C for 2 h with a heating rate of 10 °C/minunder airatmosphere. The five prepared catalysts were numberedaccording to theirFe/Ni molar ratio.That is, FeNi31-Al_2O_3, FeNi21-Al_2O_3, FeNi11-Al_2O_3, FeNi12-Al_2O_3, and FeNi13-Al_2O_3, correspond to the Fe/Ni molar ratios of 3:1, 2:1, 1:1, 1:2, and 1:3, respectively.

2.3 Synthesis ofFeNi-OCNTsElectrocatalysts

The catalytic vapor deposition method was used to produce the CNTs.The experiments were carried out in a two-stage fixed bed reactor (as shown in Figure S1) consisting of aquartz tube reactor with two heating zones (upper stage for plastic

pyrolysis, lower stage for volatile catalytic vapor deposition) that were controlled separately. In each experiment, the reactor was charged with 1 g plastic waste in a ceramic holder(upperstage) and 0.5 g Fe-Ni catalystin a stainless mesh basket (lower stage)(D. Yao et al., 2018; Yao et al., 2018a). Initially, the lower stage was preheated to 800 °C(heating rate: 20 °C/min).Once the lowerstage reached the target temperature, the waste plasticsample was pushedto the middle of the upper stage and heated to 500 °C (heating rate: 10 °C/min). The system was maintainedunder isothermalconditions for 10 min to ensure complete evolution of the volatiles. The evolving gas was adsorbed with ethanol to avoid environmental pollution. The reactions were conducted under inert atmosphere using nitrogen (99.99% purity) as the carrier gas (flow rate: 100 mL/min). The black solid containing the catalyst (lower stage) was collected and refluxed in 200 mL20 wt.% nitric acid for 4h (100°C)to remove impurities and unstable species, such as metal particles on the outer nanotube surface and part of amorphous carbon,and wassubsequentlywashed with distilled water until the pH of the filtrate was 7.The residuewas dried at 105°C for 12h. The products were numbered according to the used catalyst.For example, the product obtainedfrom FeNi31-Al_2O_3 was named FeNi31-OCNT.

2.4 Characterization of FeNi-OCNTs

The basic surface morphology of the FeNi-OCNT catalysts was studied through field scanning electronic microscope (FSEM, Nova NanoSEM 450) and transmission electron microscopy (TEM, JEM-2100F). High resolution images of the CNTs were

obtained by high-resolution transmission electron microscopy (HR-TEM) and distribution of different metals was investigated using high-angle annular dark field detector and energy dispersive spectroscopy (HAADF-STEM-EDS). The specific surface areas, pore volumes, and pore size distribution were investigatedthrough nitrogen adsorption measurement at 77 K (Quantachrome IQ)with the Brunauer−Emmett−Teller (BET) theory, v-Tmethod,and QSDFT methodsfrom 1.7 nm to 33nm. The crystalstructuresofthe CNTs were determined by X-ray diffraction (XRD) on a Philips X'Pert PRO instrumentwith a scanning step of 0.026º in the 2θ range from 5º to 85º.Raman spectroscopy was performed on a LabRAM HR800 spectrometer at a wavelength of 532 nm with Raman shift from 200 cm^{-1} to 3500 cm^{-1}.Surface chemical states were analyzed by X-ray photoelectron spectroscopy (XPS, Axis Ultra DLD, Kratos) using Al Kα line (15 kV, 10 mA, 150 W) as the radiation source.

2.5 ORR CatalyticPropertyMeasurements

The electrochemical measurements were conducted on an electrochemical workstation equipped with a rotating disk electrode (RDE, CHI760E,ATA-1B, China) in a three-electrode system.Saturated calomel and Pt wire were used as the reference and counter electrodes, respectively.The working electrode consisted of a3 mm diameter and 4 mm thickness RDE coated with aFeNi-OCNTsfilm.

FeNi-OCNTswereground for 30 min prior to preparation of the catalyst ink.For each test, 10 mg catalyst powder was dispersed in 100 μL absolute ethanol and 40 μL of 5 wt.% Nafion was added. The mixture was stirred for 30 minunder sonication, yielding a

168 homogenous ink.The working electrode was charged with 2 μL of the ink and dried
169 overnight.The ORR performance was evaluated in N_2- and O_2-saturated 0.1 M KOH
170 aqueous solutions. The obtained potentials were converted to reversible hydrogen
171 electrode using the equation

$$E(\text{vs RHE}) = E(\text{vs SCE}) + 0.0591\,\text{pH} + 0.24 \quad (1)$$

172 where RHE is the reversible hydrogen electrode, SCE is the saturated calomel
173 electrode, and pH is the hydrogen ion concentration.

174 Electron transfer number n for Fe-Ni electrocatalystswas calculated using the
175 Koutecky-Levich equation as follows

$$\frac{1}{J} = \frac{1}{J_L} + \frac{1}{J_K} = \frac{1}{B\omega^{1/2}} + \frac{1}{J_K} \quad (2)$$

$$B = 0.62nFC_0D_0^{2/3}v^{-1/6} \quad (3)$$

176 where J is the measured current density, J_K is the kinetic current density, J_L is the
177 diffusion-limited current density, ω is the electrode rotation rate,F is the Faraday
178 constant (96485 C/mol),C_0 is the bulk concentration of O_2 (1.2×10^{-3} mol/L for a 0.1 M
179 KOH aqueous solution), D_0 is the diffusion coefficient of O_2 (1.9×10^{-5} cm^2/s for a 0.1
180 M KOH aqueous solution), and v is the kinetic viscosity of the electrolyte (0.01 cm^2/s
181 for a 0.1 M KOH aqueous solution).

182 3 Results and Discussion

183 3.1Physical PorosityofFeNi-OCNTs

184 Typical FSEM images of the prepared FeNi-OCNTsare shown in Figure 1, and

185 confirm the successful synthesis of CNTs. The images reveal a fibrous structure of
186 interwoven and stacked nanotubes with diameter of approximately 20–50 nm and
187 length ranging from tens of nanometers to several micrometers, dimensions which are
188 similar to those ofCNTsprepared bycatalytic pyrolysis previously(Yao et al., 2017). The
189 small size of the CNTs imply that the enclosed metal particles are nanoscale and
190 indicate uniformity of metal particle dispersion, significant features of ORR catalysts(Ji
191 et al., 2017). Figure 1a-e shows thatiron-rich CNTsare shorter and thicker than those
192 containing a low Fe/Ni ratio. The nanotubes in FeNi12-OCNT and FeNi13-OCNT are
193 longer and thinner than those in the other three samples. It has been reported that a high
194 nickel content leads to more homogeneous and longerCNTs, which is possibly a result
195 of better dispersion of smaller metal particles owing to the stronger interaction between
196 the nickel metalparticles and the support, andconfirms that the CNTs morphology is
197 related to the particle size of the catalyst(Chung et al., 2005).
198 Theisothermaladsorptionprofileofthe solidcarbonmaterialsshown in Figure 2a reveals
199 that all FeNi-OCNTs exhibit reversible type IV isotherm and H3 hysteresis loops, the
200 latter at 0.5–1.0 relative pressure, which is themain characteristic of mesoporous
201 materials. The calculated specific surface areas of FeNi31-OCNT, FeNi21-OCNT,
202 FeNi11-OCNT, FeNi12-OCNT, and FeNi13-OCNTare134.6 m^2/g, 162.3 m^2/g,120.4
203 m^2/g, 134.6 m^2/g, and 126.4m^2/g, respectively. Pore volumes and average diameters of
204 the FeNi-OCNTsare given in Table S2, and indicate that FeNi21-OCNTexhibits the
205 highest total pore volume and average diameter. The pore size distribution, displayed in
206 Figure 2b, shows thatall FeNi-OCNTs exhibit four distinguished mesopore distribution

207 peaks at around 9.6 nm, 11.5 nm, 15.0 nm, and 26.1 nm, and that the occurrence of
208 smaller pores correlates with an increase in the nickel content, which is consistent with
209 the SEM results. The mesoporousstructure of the catalystsprobably corresponds to the
210 inner diameter of the CNTs. Of note, substantial catalyst mesoporosityis regarded as
211 ideal for the ORR, as it correlates with fast mass-transport in theelectrolytes and high
212 exposure of active sites(Zhang et al., 2018).

213 **3.2 Chemical Structure ofFeNi-OCNTs**

214 From theTEM images of FeNi12-OCNT,it can be observed that the metal
215 nanoparticles are encapsulated in the CNTs(Figure 3a, b). The HR-TEM images reveal
216 that the outer diameter of FeNi12-OCNT rangesfromabout 10nm totens of
217 nanometers,and that the metalnanoparticles of ~20nm size are wrapped in ~10nm thin
218 carbon layers (Figure 3b, c). Furthermore, the HR-TEM imagefor single tubein Figure
219 3c indicates that the 0.202 nm nanoparticle lattice fringe is associated with the(111)
220 plane of $FeNi_3$alloy.The TEM–energy-dispersive X-ray (TEM-EDX) shows that
221 FeNi12-OCNT is composed of C with encapsulatedFe-Ni alloy nanoparticles (Figure
222 3d, e, f).The linear profiles obtained by HAADF–STEM of a single particle (Figure 3d,
223 inset) show higher intensity for Ni than Fe,which indicates the presence of more Ni
224 atoms (Figure 3g). And the exact content of the two metals will be studied in the future
225 according to these works (Pierce et al., 1998; Yang et al., 2010).

226 The Raman spectra ofFeNi-OCNTsshow three characteristic bands at around 1340
227 cm^{-1} (D band), 1580 cm^{-1} (G band), and 2670 cm^{-1} (G' band, Figure 4a), which

correspond to the defects in graphene, the planar motion of sp^2-hybridized carbon atoms in the graphite layers, and the ejection scattering of the two phonons, respectively. The I_D/I_G ratio is commonly used to describe the degree of structural defects of carbon materials. The I_D/I_Gratios for FeNi31-OCNT, FeNi21-OCNT, FeNi11-OCNT, FeNi12-OCNT, FeNi13-OCNT are 0.78, 0.75, 0.82, 0.72, and 0.79, respectively, and are comparable with the values of OCNTs used in commercial applications andthose reported in theliterature(Kaushik et al., 2014; Wang et al., 2018). In addition, the ratio $I_{G'}/I_G$ can be used to describe the purity of the CNTs.In this study, the obtained valuesin the range 0.38–0.50 indicate that the synthesized catalysts have a high degree of graphitization.Moreover, $I_{G'}/I_G$sank from 0.49 to 0.38 with the decrease in the Fe/Ni ratio from 3:1 to 1:1, indicatinga gradual decrease in the CNTpurity with the amount of Fe, until a ratio Fe/Ni of 1:3 at which point $I_{G'}/I_G$ increased to 0.50.

The sharp graphite peaks at 2θ ~26º in the XRD patterns ofall FeNi-OCNT catalysts (Figure 4b)correspond to the (002) facets of graphite carbon and suggest a high degree of graphitization, which could stem from the CNTsand Fe-Ni alloys. A high degree of graphitization corresponds to good electrical conductivity, which is beneficial to electrochemical applications. In particular, the lower angle of the (002) peak of FeNi12-OCNT indicates a larger inter-layer spacing. This could be explained by theattack of the defective sites by nitric acid, which could intercalate into the CNTs to unzip the tube walls,thus increasing exposure of the active sites(Zhao et al., 2006). The peaks observed at 43º and 75ºconfirm the presence of a Fe-Ni alloy,which is in accordance with the TEM results. Furthermore, Fe_3C found in the catalystswas

250 generatedduring the growth of the CNTs(Yao et al., 2018a) and could either serve as an
251 efficient catalytic site(Yang et al., 2015) or boost the activity of other catalytic
252 sites(Jiang et al., 2016). In addition, the detection of residualAl_2O_3 (2θ=67°)implies that
253 it was not entirely removed during concentrated nitric acid washing because ofits high
254 stability.

255 XPScharacterization was carried out to furtherdetermine the components in the
256 prepared composites. As displayed in Figure 5a, the wide-scan spectrum indicates that
257 FeNi-OCNTs mainly consisted of C and O,and peaks corresponding to Fe and Ni were
258 not observed. As shown in Table S3, the amount of C decreased while that of O
259 increased with the rise in the Ni ratio. Only few Fe and Ni atoms were observedon the
260 surface of the samples. These results are confirmed by the XPS spectrum of
261 FeNi12-OCNT shown in Figure 5b.The removal of Ni and Fe from the CNT surface by
262 refluxing with concentrated nitric acid aims at the enhancement of catalyst stability by
263 preventing the direct reaction of the surface-bound metal with electrolyte. Taking
264 FeNi12-OCNTas an example, the C 1s XPS spectrum in Figure 5c shows an intense
265 signal at 285 eV, which corresponds to the graphitic structure (sp2 hybridization) of the
266 FeNi-OCNTs, and a signal at 285.6 eV,which results from structural defects(Datsyuk et
267 al., 2008). Furthermore,the three signals at 286.4 eV, 287.2 eV, and 289.7 eV
268 correspond to oxygen-bound carbon atoms and can beattributedtoC-O-C (mainly from
269 phenols), C=O, and -COOH (mainly from carboxylic acids), respectively(Zhang et al.,
270 2008), whereas the–COOH groups were likely formed during thetreatment
271 withconcentrated nitric acid(Savilov et al., 2010). The presence of these

oxygen-containinghydrophilic groupsimproves the dispersion of theCNTsin water(Hiura et al., 1995), and thereforefavorsthe exposure of the catalytic active sites.Figure 5d shows the O 1s spectra of FeNi12-OCNT. The peaks at 532.8 eV, 534.3 eV, and 536 eV correspond to C=O, C-O, and -COOH, respectively.These functional groups can facilitate the O_2 adsorption and the following O_2 reduction reaction, resulting in improvedelectrocatalytic performance of the material.In addition, the peak at 537.6 eV corresponds to chemisorbed H_2O (or H-O-H)(Chiang et al., 2011).

3.3ORRproperties

Cyclic voltammetry (CV) results of the FeNi-OCNTs samples are shown in Figure 6a. In contrast to themeasurements in N_2-saturated electrolytes, those in an O_2-saturated electrolytefeature sharp reduction peaks in their CV curves, suggestingdistinct catalytic activity for the oxygen reduction reaction. In addition, the reduction peak potential of FeNi-OCNTsshifted from0.77 V to 0.87 V with the increase in the nickel content from 25% to 66%, and subsequently decreased to 0.85V.Linear sweep voltammetry (LSV) of all samples in the O_2-saturated 0.1M aqueous KOH electrolyte were recorded at 10 mV/sand 1600 rpm. The electrocatalytic activities of the five catalysts and commercial 20% Pt/C(Figure 6b) reveal that the ORR shift of the onset and half-wave potentials to more positive values coincide with the increase in the ratio of Ni in the catalyst, whereas higher positive potentials suggest an effectively enhanced ORR activity. More specifically, the onset and the half-wave potential increased from 0.94V to 1.01V and from 0.79 V to 0.88 V, respectively, with the increase in Ni/Fe ratio (Table S4), and the

highest positive potentials were observed for the FeNi12-OCNT catalyst. In addition to the onset and half-wave potentials, the limiting diffusion current also varies with the ratio of Ni in the catalysts. FeNi12-OCNT shows more stablelimiting current than the other tested catalystsat the diffusion-controlled region, and its performance was remarkably close to that of the commercial 20% Pt/C catalyst.

The Fe-Ni alloy play a crucial role in the enhanced electrocatalytic activity ofFeNi-OCNTsin the ORR in analkaline solution. LSV of FeNi12-OCNTwas measured at rotation rates in the range 800–2000rpm (Figure 6c), and show thatthe limited current density increases with the rotation rate as a result of the faster oxygen diffusion to the catalysts. In Figure 6d, the fitting curves of Koutecky-Levich (K-L) plotsobtained at different potentialsshow nearly linear relationships, whichindicate the first-order reaction kineticswith regard to the O_2concentration in the solution (Dey et al., 2014). The inset inFigure 6dhighlights the change in the electron transfer numbers (n) calculated from K-L plots from 3.79 to 3.98 over the potential range 0.3–0.6 V.Notably, these are close to the theoretical value of 4.The electron transfer numbers of the other catalysts were estimated from the K−L plots and are shown in Figure S2. In conclusion, the Fe-Ni-bimetallic-loaded CNT catalystsdisplay superior oxygen reduction reaction performanceunder theseconditions.

High electrocatalytic activity in the ORR is not the onlyassessment criterion for the replacement of Pt/C byFeNi-OCNTs as cathodic catalystsin commercial fuel cells.Long-term stability and methanol tolerance are equally importantfor the estimation of the ORR performance in practical applications. Firstly, the durability was

evaluated by chronoamperometry in O_2-saturated 0.1M aqueous KOH at 0.6V. As shown in Figure 7a, the FeNi12-OCNT material show superior electrochemical durability to the 20% Pt/C catalyst, retaining 97.6% of the initial current after 40000s of continuous operation in contrast to 95.3% retained by Pt/C under the same conditions.It is known that Pt/C deactivation is due to the loss, susceptible oxidation, or agglomeration of Pt nanoparticles, as well as the corrosion of the carbon black support. Next, the methanol tolerance of FeNi12-OCNT and Pt/C were assessed in O_2-saturated 0.1 M aqueous KOH containing 3 M methanol, as the methanol poisoning of catalysts is another important aspect of practical applications. As shown in Figure 7b, a sharp current drop of over 10% of the initial current was observed in the chronoamperogram of the commercial 20% Pt/C electrocatalyst in the presence of methanol. In contrast, the FeNi12-OCNTs exhibit high methanol tolerance with only a slight decrease in the current upon addition of methanol, which indicates that the 20% Pt/C electrocatalyst is farmore prone to methanol poisoning thanFeNi12-OCNT.As illustrated in Figure 8, the long-term stability and methanol tolerance of FeNi12-OCNTresult from the unique structure ofthe synthesized CNT materials, in which the encapsulated alloy particles are protectedfromaggregation andcorrosion(Lai et al., 2018).The significant advantages of the prepared catalysts,such as higher stability and methanol tolerance, render them promising candidates for application in the catalytic oxygen reduction reaction.

4 Conclusion

A cost-effective method for the transformation of plastic wasteintohighly efficient

electrocatalystsby a catalytic pyrolysis process has beendeveloped. The variation of the Fe/Ni ratio has a significant impact on the physicochemical properties of the obtained FeNi-OCNTs. While a lowerFe/Ni ratiocan lead tolonger,smoother CNTswith narrower mesopores, theC/O surface-mass ratio of FeNi-OCNTs increases with the rise in the Fe/Ni ratio.FeNi-OCNT with a Fe/Ni ratio of 1:2exhibitedremarkable ORR catalytic activity, which is comparable to that ofa commercial 20% Pt/C catalyst.The onset and half-wave potentials of FeNi12-OCNT were lower than those of the commercial 20% Pt/C catalyst by only 30 mV and 20 mV, respectively. In addition, FeNi12-OCNTshowed superior durability and methanol tolerance in an alkaline solution. The outstanding electrocatalytic performance was attributed to the co-existence of the bimetallic Fe-Ni alloy, Fe_3C, and oxygen-containing functional groupsinthe FeNi-OCNTs. This study not only provides a novel method to reutilize plastic waste, but alsobroadens the design strategies for low-cost, high-performance nonprecious catalysts with controllable bimetallic-species-loaded carbon-based materials.

Acknowledgements

The authors wish to express their sincere thanks forthe National Key Research and Development Program of China (2018YFC1901204)and the financial support from the National Natural Science Foundation of China(51622604and51806077). The experiment was also assisted by the Analytical and Testing Center in Huazhong University of Science & Technology (http://atc.hust.edu.cn, Wuhan 430074 China).We

also would like to thank Editage (www.editage.cn) for English language editing.

Competing interests

The authors declare no competing financial interests with others.

Reference

Aboul-Enein, A.A., Awadallah, A. E. 2018. Production of nanostructuredcarbon materials using Fe–Mo/MgO catalysts via mild catalytic pyrolysis ofpolyethylenewaste.*Chem.Eng.J.*, **354**,802-816.https://doi.org/10.1016/j.cej.2018.08.046.

Bientinesi, M., Petarca, L. 2009. Comparative environmental analysis of wastebrominated plastic thermaltreatments. *Waste Manage.*, **29**(3), 1095-102.https://doi.org/10.1016/j.wasman.2008.08.004.

Caroline, A.P., B. 2018. China's plastic waste import ban. *Science*, **360**(6395),1310. https://doi.org/10.1126/science.360.6395.1310-b.

Chiang, Y., Lin, W., Chang, Y. 2011. The influence of treatment duration onmulti-walled carbon nanotubes functionalized by H_2SO_4/HNO_3 oxidation. *Appl.Surf. Sci.*, **257**, 2401–2410. https://doi.org/10.1016/j.apsusc.2010.09.110.

Chung, Y., Jou, S.2005. Carbon nanotubes from catalytic pyrolysis ofpolypropylene.*Mater.Chem.Phys.,***92**,256–259.https://doi.org/10.1016/j.matchemphys.2005.01.023.

Ding. Y, Ye. Z., Poul. W, Hao. Y, Han, C. 2018. Co-production of hydrogen andcarbon nanotubes from real-world waste plasticsInfluence of catalyst composition and operational parameters. *Appl. Catal. B: Environ.*, **221**, 584–597.https://doi.org/10.1016/j.apcatb.2017.09.035.

Datsyuk, V., Kalyva, M., Papagelis, K. Parthenios, J. Tasis, D., Siokou, A.,Kallitsisa, I.,

Galiotis, C. 2008. Chemical oxidation of multiwalled carbonnanotubes. *Carbon*, **46**, 833-840. https://doi.org/10.1016/j.carbon.2008.02.012.

De, S., Zhang, J., Luque, R.,Yan, N. 2016. Ni-based bimetallicheterogeneous catalysts for energy and environmental applications. *EnergyEnviron. Sci.*, **9**, 3314--3347. https://doi.org/10.1039/C6EE02002J.

Dey, S., Rana, A., Crouthers, D., Mondal, B., Das, P., Darensbourg, M. Y.,Dey, A. 2014. Electrocatalytic O_2 Reduction by [Fe-Fe]-Hydrogenase Active Site Models.*J.Am.Chem.Soc*., **136**,8847-8850. https://doi.org/10.1021/ja5021684.

Ferrandon, M., Wang, X., Kropf, A. J. D., Myers, J. Wu, G. Johnston,C. M.,Zelenay,P.2013. Stability ofironspeciesin heat-treatedpolyaniline–iron–carbonpolymerelectrolytefuelcellcathodecatalysts.*Electrochim.Acta,***110**, 282-291. https://doi.org/10.1016/j.electacta.2013.03.183.

Geyer, R., Jambeck, J. R., Law, K. L. 2017. Production, use, and fate of allplastics ever made. *Sci. Adv.*, **3**, 1-5. https://doi.org/10.1126/sciadv.1700782.

Hiura, H., Ebbesen, T., Tanigaki, K. 1995. Opening and Purification ofCarbonNanotubesinHighYields.*Adv.Mater.,***7**(3),275-276.https://doi.org/10.1002/adma.19950070304.

Ji, D., Peng, S., Safanama, D., Yu, H., Li, L., Yang, G., Qin, X., Srinivasan,M.,dams, S., Ramakrishna, S. 2017. Design of 3-Dimensional HierarchicalArchitectures of Carbon and Highly Active Transition Metals (Fe, Co, Ni) asBifunctional Oxygen Catalysts for Hybrid Lithium–Air Batteries. *Chem. Mater.*,**29**(4), 1665-1675. https://doi.org/10.1021/acs.chemmater.6b05056.

403

404 Jiang, W., Gu, L., Li, L., Zhang, Y., Zhang, X., Zhang, L. Wang, J., Hu, J.,Wei,Z.,

405 Wan, L. 2016. Understanding the High Activity of Fe-N-CElectrocatalysts in

406 Oxygen Reduction: Fe/Fe_3C Nanoparticles Boost theActivityof Fe-N(x).

407 *J.Am.Chem.Soc.*, **138**(10),3570-8. https://doi.org/10.1021/jacs.6b00757.

408 Jonathan, A.W., C., Williams, P.2016. The use of different metal catalysts for the

409 simultaneous production of carbon nanotubes and hydrogen from pyrolysisof

410 plasticfeedstocks.*Appl.*

411 *Catal.B:Environ.*,**180**,497-510.https://doi.org/10.1016/j.apcatb.2015.06.054.

412 Kaushik, V., Shukla,A.,Vankar, V. 2014. Microwave plasma

413 CVD-growngraphene–CNT hybrids for enhanced electron field emission applications.

414 *Appl.Phys.A: Mater.Sci.Process.*,**117**,

415 2197–2205.https://doi.org/10.1007/s00339-014-8646-2.

416 Kong, J., Cassell, A. M.,Dai, H. . 1998. Chemical vapor deposition of methanefor

417 single-walled carbon nanotubes. *Chem. Phys. Lett.,***292**,

418 567–574.https://doi.org/10.1016/s0009-2614(98)00745-3.

419 Lai, C.W., J., Lei, W.,Xuan, C.,Xiao, W., Zhao,T., Huang,T.,Chen,L.,Zhu,Y.,Wang,

420 D. . 2018. Restricting Growth of Ni_3Fe Nanoparticles onHeteroatom-Doped Carbon

421 Nanotube/Graphene Nanosheets as Air-ElectrodeElectrocatalyst for Zn-AirBattery.

422 *ACSAppl.Mater.Interfaces,***10**,38093-38100.

423 https://doi.org/10.1021/acsami.8b13751.

424 Lai, J.L., F. Tang,Y.Zhou, P. Chao, Y. Zhang, Y.Guo, S. 2019. EfficientBifunctional

425 Polyalcohol Oxidation and Oxygen Reduction ElectrocatalystsEnabled by Ultrathin
426 PtPdM (M = Ni, Fe, Co) Nanosheets. *Adv. Energy Mater.*,**9**(8), 1800684.
427 https://doi.org/10.1002/aenm.201800684.
428 Ochoa, A., Barbarias, I., Artetxe, M., Gayubo, A., Olazar, M., Bilbao, J.,Castaño, P.
429 2017. Deactivation dynamics of a Ni supported catalyst during thesteam reforming
430 of volatiles from waste polyethylene pyrolysis. *Appl. Catal. B: Environ.*,**209**,554-565.
431 https://doi.org/10.1016/j.apcatb.2017.02.015.
432 Okpalugo, T., Papakonstantinou, P., Murphy, H., McLaughlin, J.,Brown, N. 2018.
433 Principles of Catalysis with Application in Energy Conversion. *Carbon*,**43**.
434 https://doi.org/10.1016/j.carbon.2004.08.033.
435 Pierce C., Adams K., Stewart J., 1998.Determining the Fuel Constituents of Ancient
436 Hearth Ash Via ICP-AES Analysis. *J. Archaeol. Sci*., **25**, 493-503.
437 https://doi.org/10.1006/jasc.1997.0252.
438 Savilov S., Cherkasov N., Kirikova M., Ivanov A. Lunin V. 2010. Multiwalled carbon
439 nanotubes and nanofibers: similarities and differences from structural, electronic and
440 chemical concepts; chemical modification for new materials design. *Funct. Mater. Lett.*,
441 **3**, 289-294. https://doi.org/10.1142/S1793604710001421.
442 Sharuddin, S., Abnisa, Daud, F. W., Aroua, M. 2016. A review on pyrolysis
443 ofplasticwastes.*EnergyConvers.Manage.,***115**,308-326.https://doi.org/10.1016/j.encon
444 man.2016.02.037.
445 Shen, Y., Zhao, P., Shao, Q., Ma, D., Takahashi,F.,Yoshikawa, K. 2014.In-situ catalytic
446 conversion of tar using rice husk char-supported nickel-iron catalystsforbiomass

pyrolysis/gasification. *Appl. Catal. B: Environ.*, **152**,140-151. https://doi.org/10.1016/j.apcatb.2014.01.032.

S.M. Al-Salema, A. Antelava, A. Constantinou, G. Manos, A. Dutta, 2017. A review on thermal and catalytic pyrolysis of plastic solid waste (PSW) J. Environ. Manage. 197, 177-198. https://doi.org/10.1016/j.jenvman.2017.03.084

Stamenkovic, V.R.F., B. Mun, B. Wang, G. Ross,P. N. Lucas, C. A. Marković,N. M. 2007. Improved Oxygen Reduction Activity on $Pt_3Ni(111)$ via IncreasedSurfaceSiteAvailability. *Science*, **315**(5811),493-497.https://doi.org/10.1126/science.1135941.

Wang, Y., Wang, L.,Tong, M., Zhao,X., Gao, Y.,Fu, H. 2018. Co-VNencapsulated in bamboo-like N-doped carbon nanotubes for ultrahigh-stabilityof oxygen reductionreaction. *Nanoscale*,**10**(9),4311-4319. https://doi.org/10.1039/c7nr09538d.

Wu, C., Williams, P. T. 2009. Hydrogen production by steam gasification ofpolypropylene with various nickel catalysts. *Appl. Catal. B: Environ.*,**87**(3-4), 152-161. https://doi.org/10.1016/j.apcatb.2009.03.004.

Yang, W., Liu, X., Yue,X.,Jia, J., Guo, S. 2015. Bamboo-like carbonnanotube/Fe_3C nanoparticle hybrids and their highly efficient catalysis foroxygenreduction.*J.Am.Chem.Soc.*, **137**(4), 1436-9. https://doi.org/10.1021/ja5129132.

Yang K., Kitto M., Orsini J., Swami K., Beach S. 2010. Evaluation of sample pretreatment methods for multiwalled and single-walled carbon nanotubes for the

469 determination of metal impurities by ICPMS, ICPOES, and instrument neutron
470 activation analysis.*J. Anal. At. Spectrom*. 25, 1290-1297.
471 https://doi.org/10.1039/C0JA00012D.
472 Yao, D., Zhang, Y,. Williams, P.T., Yang, H., Chen, H. 2018a. Co-productionof
473 hydrogen and carbon nanotubes from real-world waste plastics: Influence
474 ofcatalystcomposition and operational parameters. *Appl. Catal. B: Environ.*,**221**,
475 584-597. https://doi.org/10.1016/j.apcatb.2017.09.035.
476 Yao, D., Wu, C., Yang, H., Zhang, Y., Nahil, M. A., Chen, Y., Williams,P. T.,Chen, H.
477 2017. Co-production of hydrogen and carbon nanotubes fromcatalytic yrolysis of waste
478 plastics on Ni-Fe bimetallic catalyst. *EnergyConvers.*
479 *Manage.*,**48**,692-700.https://doi.org/10.1016/j.enconman.2017.06.012.
480 Yao, D., Yang, H.,Chen, H., Williams, P. 2018b. Co-precipitation,impregnation and
481 so-gel preparation of Ni catalysts for pyrolysis-catalytic steamreforming of
482 wasteplastics. *Appl. Catal. B:*
483 *Environ.*,**239**,565-577.https://doi.org/10.1016/j.apcatb.2018.07.075.
484 Zhang, C., Liu, J., Ye, Y., Aslam, Z., Brydson, R., Liang, C. 2018.
485 Fe-N-dopedmesoporous carbon with dual active sites loaded on reduced graphene
486 oxides forefficient oxygen reduction catalysts. *ACS Appl. Mater. Interfaces*, **10**,
487 2423-2429.https://doi.org/10.1021/acsami.7b14443.
488 Zhang, G.,Sun,S.,Yang, D., Dodelet, J., Sacher, E. 2008. The surfaceanalytical
489 characterization of carbon fibers functionalized by H_2SO_4/HNO_3 treatment.*Carbon*,**46**,
490 196-205. https://doi.org/10.1016/j.carbon.2007.11.002.

Zhao,N.,He, C., Li, J., Jiang, Z., Li, Y. 2006. Study on purification andtip-opening of CNTs fabricated by CVD. *Materials Research Bulletin*, **41**(12),2204-2209. https://doi.org/10.1016/j.materresbull.2006.04.029.

Zhao, X., Chen, S., Fang, Z., Ding, J., Sang, W., Wang, Y., Zhao, J., Peng,Z., Zeng, J. 2015. Octahedral Pd@$Pt_{1.8}$Ni core-shell nanocrystals withultrathin PtNi alloy shells as active catalysts for oxygen reduction reaction. *J.Am. Chem. Soc.*, **137**(8), 2804-2807. https://doi.org/10.1021/ja511596c.

Zhao, Y., Lv, X., Ni, H. 2018. Solvent-based separation and recycling of wasteplastics: Areview.*Chemosphere*,**209**,707-720.https://doi.org/10.1016/j.chemosphere.2018.06.095.

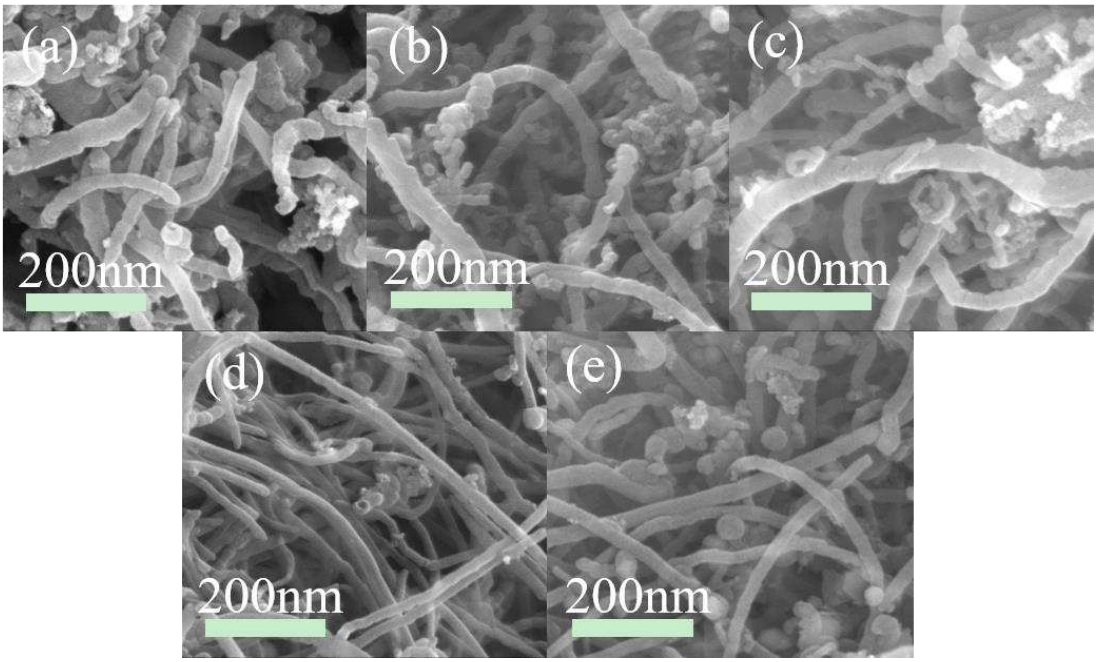

Figure 1 FSEM images of (a) FeNi31-OCNT, (b) FeNi21-OCNT, (c) FeNi11-OCNT, (d) FeNi12-OCNT, and (e) FeNi13-OCNT.

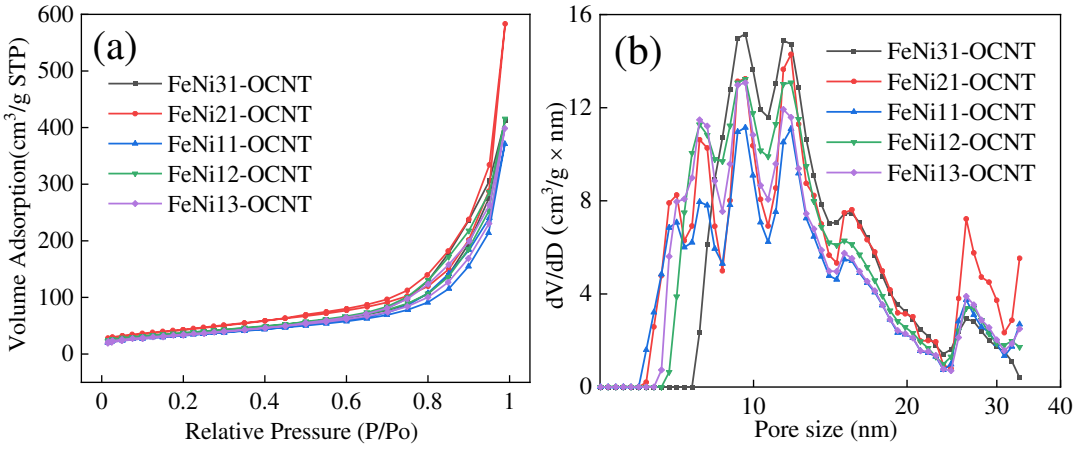

Figure 2 (a) N_2 adsorption/desorption isotherms of FeNi-OCNTs. (b) Pore distribution of FeNi-OCNTs.

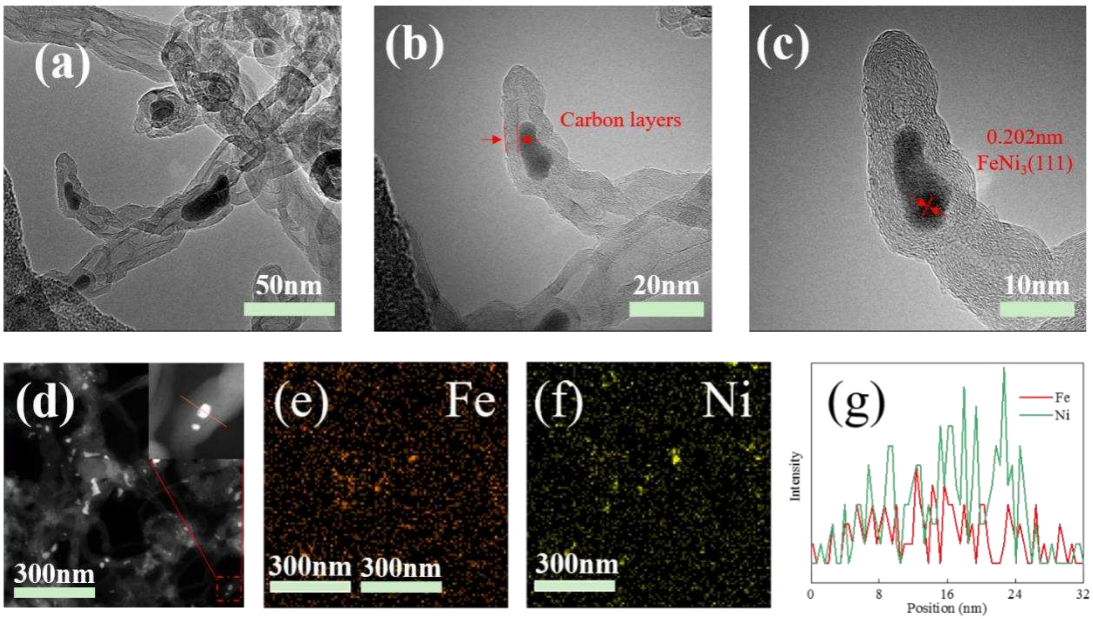

Figure 3 (a)TEM image of FeNi12-OCNT. (b) HR-TEM of Fe-Ni alloy inside. (c) HR-TEM image showing the presence of Fe-Ni alloy. (d) HAADF–STEM images with elemental mapping of Fe (e) and Ni (f). (g) HAADF–STEM cross-sectional compositional profiles.

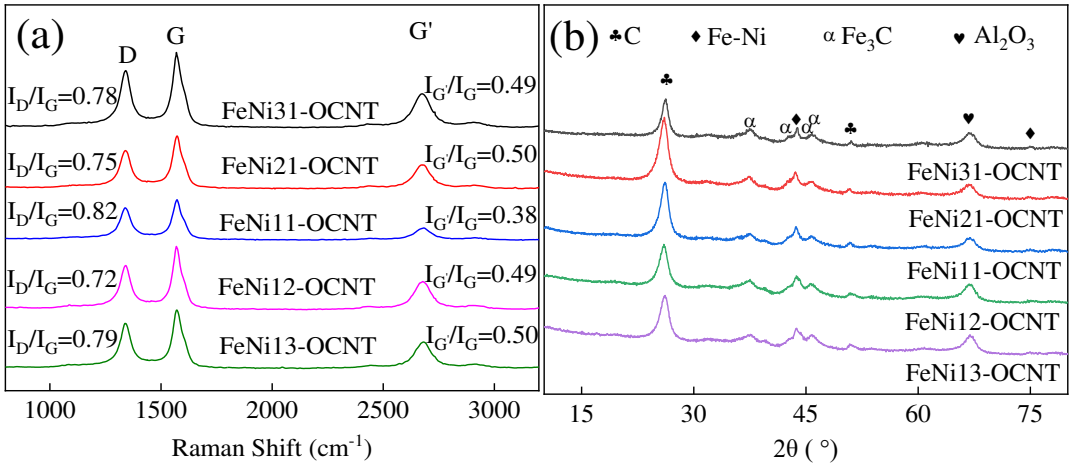

Figure 4 (a) Raman spectra of FeNi-OCNTs. (b) X-ray diffraction patterns of FeNi-OCNTs.

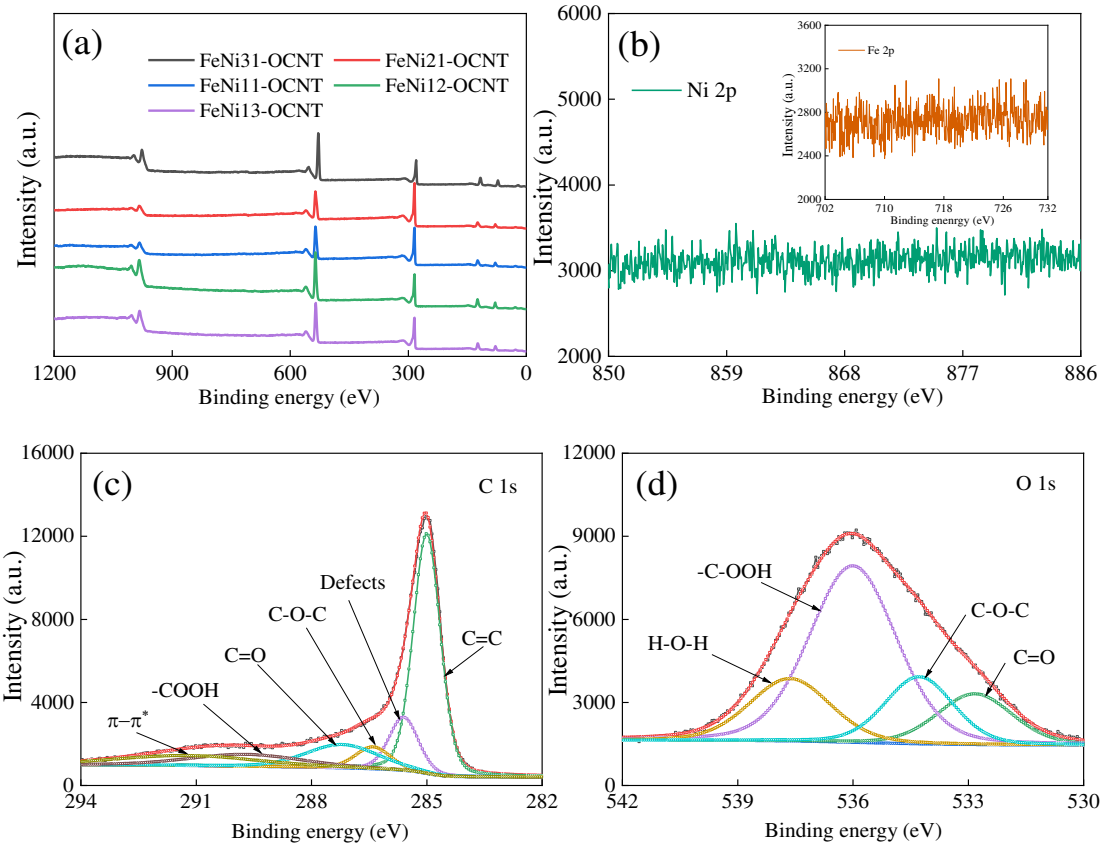

Figure 5 (a) XPS survey spectrum of FeNi-OCNTs and (b) high-resolution XPS spectrum of Ni 2p and Fe 2p of the FeNi12-OCNT sample. (c) XPS spectrum of C 1s of the FeNi12-OCNT sample. (d) XPS spectrum of O 1s of the FeNi12-OCNT sample.

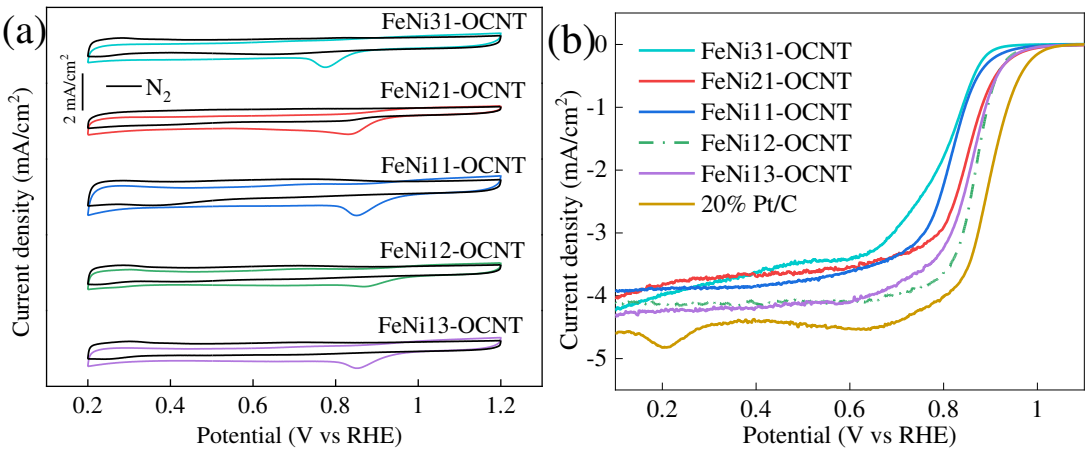

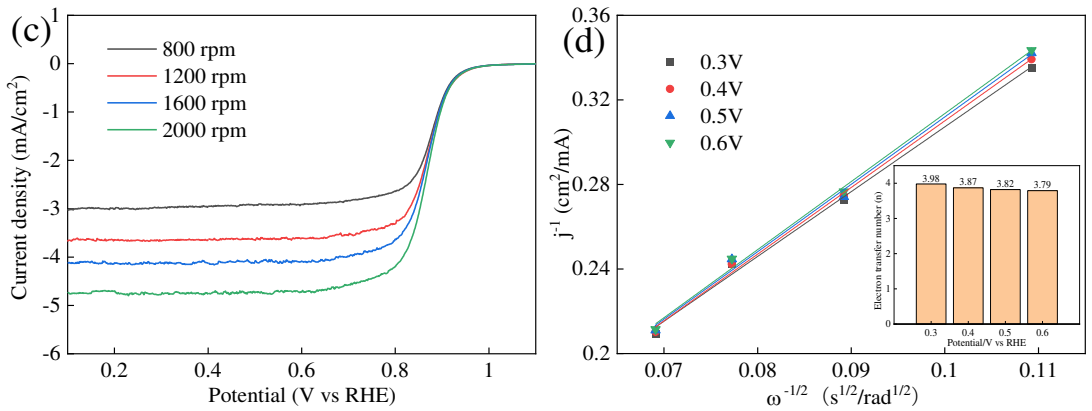

524

525 Figure 6 (a) CV curves of the FeNi-OCNTs and of 20% Pt/C in O_2-saturated 0.1 M
526 KOH aqueous solutions at 10 mV/s scan rate. (b) LSV curves of FeNi-OCNTs and of
527 20% Pt/C in O_2-saturated solutions at 5 mV/s scan rate and 1600 rpm rotation speed. (c)
528 LSV curves of FeNi12-OCNT at different rotation rates. (d) K–L plots of
529 FeNi12-OCNT at different potentials.

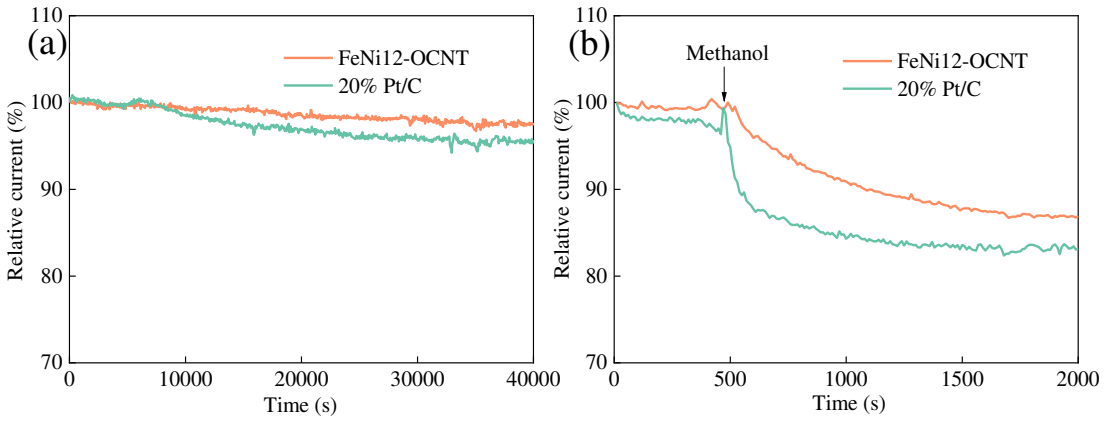

530

531 Figure 7 (a) Chronoamperometric responses of FeNi12-OCNT and 20% Pt/C in
532 O_2-saturated 0.1 M aqueous KOH at 0.6 V and 1600 rpm rotation rate. (b)
533 Chronoamperometric responses of FeNi12-OCNT and 20% Pt/C in O_2-saturated 0.1 M
534 aqueous KOH at 0.6 V with and without methanol.

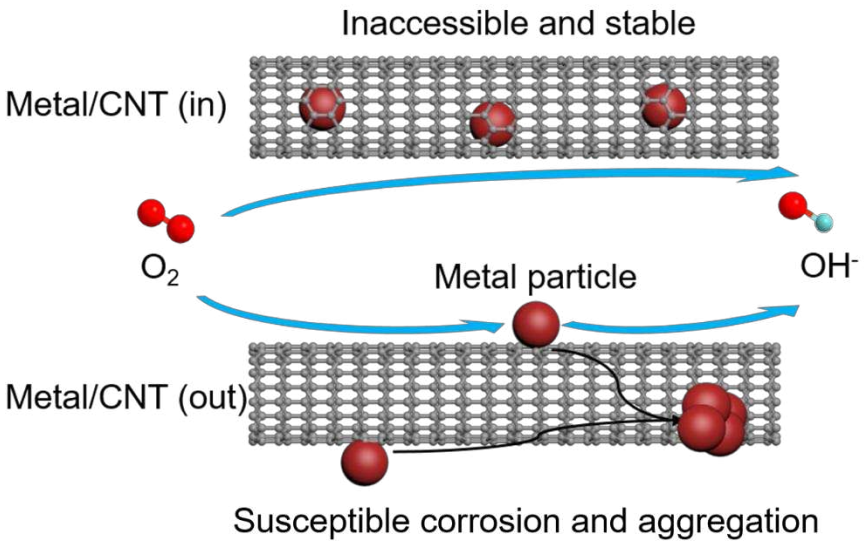

535

536 Figure 8 Schematic illustration highlighting the origin of stability.